



**Project Title:**

NeTS: Small: RUI: Bulldog Mote- Low Power Sensor Node and design Methodologies for Wireless Sensor Networks

**Energy Harvesting Technologies**

**PD/PI Name:**

Nan Wang, Principal Investigator

Woonki Na, Co-Principal Investigator: Lead Energy Harvesting Team

**Recipient Organization:**

California State University-Fresno Foundation

**Team Members:**

Maen Marji, Cheaheng Lim, and Honorio Martinez

**Project/Grant Period:**

10/01/2018 - 09/30/2021

**Reporting Period:**

10/01/2019 - 09/30/2020

Prepared by Woonki Na

## **ABSTRACT**

This report is for the energy harvesting activities in the project, 2019~2020. This report will be divided by three sections. The first one is “Sliding Mode Control based Multi-Source Energy Harvesting For Low Power Applications,” and the second part is “Development of Artificial Neural Network Based Maximum Power Point Tracking Algorithm for a Photovoltaic Application,” and the last one is “Sliding Mode Control Based Battery Management for Energy Harvesting.”

## TABLE OF CONTENTS

1. Sliding Mode Control based Multi-Source Energy Harvesting	
1.1 Overall System	2
1.2 DC/DC Converter For The Energy Harvesting	2
1.3 Sliding Mode Control For the Energy Harvesting	3
1.4 Simulation and Experimental Results	4
1.5 Conclusion and Future Works	9
2. Sliding Mode Control Based Battery Management for Energy Harvesting	10
2.1 Battery Management system	10
2.2 Constant current and constant voltage controller	10
2.2.1 Constant voltage controller	11
2.2.2 Constant current controller	12
2.3 Simulation and Experimental Results	13
2.1 Conclusion and future works	16
3. Development of Artificial Neural Network Based Maximum Power Point Tracking Algorithm for a Photovoltaic Application	
3.1 Artificial Neural Network(ANN) based MPPT	17
3.2 Simulation results	18
3.3 Conclusion and future works	20
References	21
Appendix	23

During 2019~2020, the main activities regarding energy harvesting for the project are developing the power management algorithms as follows:

## 1. Sliding Mode Control based Multi-Source Energy Harvesting

### 1.1 Overall System

The overall system topology is shown in Fig. 1.1. The system consists of a photovoltaic panel, wind turbine, piezoelectric string, and power stage for each energy source and it consists of buck-boost for the solar panel and buck converter for both wind and piezoelectric sources. Also, a battery and wireless sensor are used as a load. Controller and power management generates the control signals required to maintain the system stability, efficiency, and protection by monitoring and sensing all the system components.

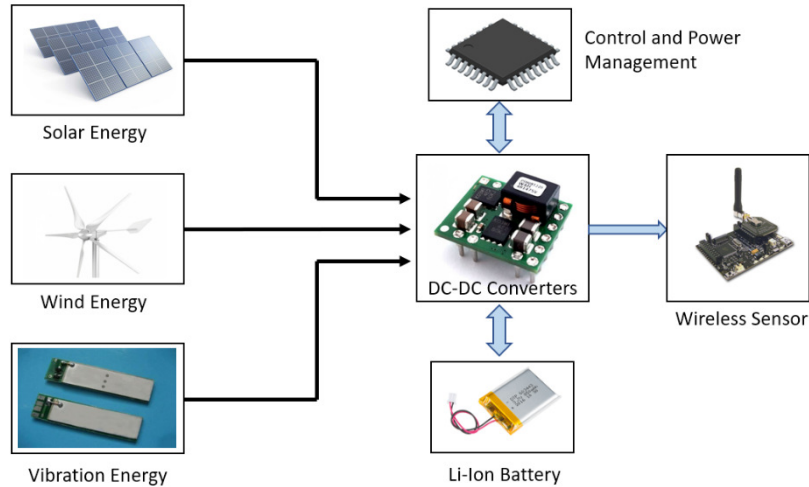


Fig.1.1 System Block Diagram.

### 1.2 DC/DC Converter For The Energy Harvesting

The output voltage equation for the 2-switch non-inverted buck-boost converter is (1.1).

$$V_o = \frac{d1}{1-d2} V_{in} \quad (1.1)$$

Where  $d1$  is the duty cycle for the buck converter and  $d2$  is the duty cycle for the boost converter. To make the converter work in a more stable way, adapt the change in inputs such as solar panels, wind turbines, etc., or the change in the load such as the case in charging a battery. The controller for 2-non inverting buck-boost converter overall schematic is also shown in Fig. 1.2.

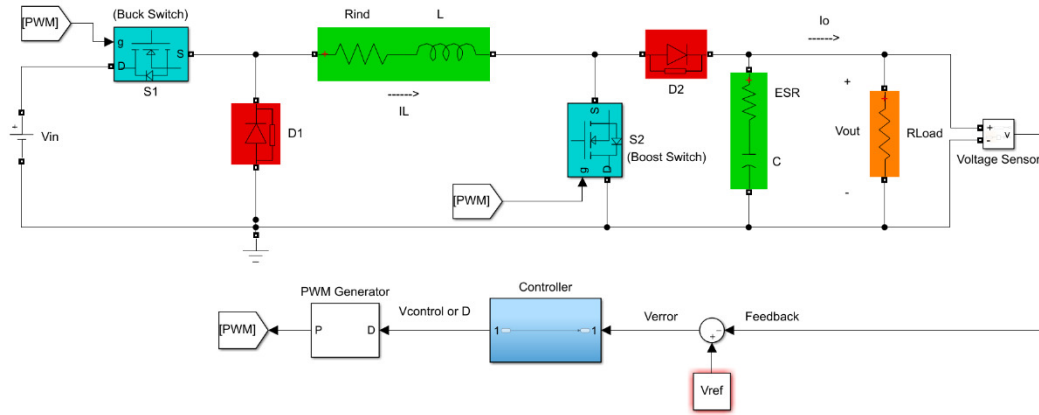


Fig. 1.2 Non Inverting buck-boost converter with a controller

Table 1 shows the power stage requirements for the solar panel circuit. Based on the calculated value of the inductor, the system should always work on Continuous Conduction Mode (CCM) unless the output power of the solar panel or the wind turbine becomes small to the point of pushing the inductor current to reach zero at the discharging period (off period). However, the controller will always adjust the duty ratio in a way that keeps tracking the maximum power point. The maximum inductor current is 1.25 A where the MOSFET must be chosen to handle this current at 100 kHz.

TABLE I. SYSTEM REQUIREMENTS.

<b>Requirements</b>	<b>Values</b>
$V_{in}$ (range)	2 - 6.5 V
$V_o$	4.2 V
$\Delta I_{Lripple}$	0.2 A or 20%
$\Delta V_{Cripple}$	0.01 or 1%

Two PID controllers have been designed and tuned, where one of them used to hold a constant voltage, while the other is used to hold a constant current. Therefore, the incremental conductance technique is used to track the maximum power point of the solar panel and then add the adjustment needed to the reference voltage or current. However, each PID controller is then connected to an inner loop SMC inductor ripple current controller.

### 1.3 Sliding Mode Control for the energy harvesting

Sliding mode control (SMC) is used to control systems that have nonlinearity in nature such as controlling switching schemes for a DC-DC converter. Also, SMC can control systems governed by ordinary differential equations with discontinuous right-hand side [1.1]. Thus, SMC has proved to be efficient with such complex systems where the implementation is simple and not expensive. Therefore, a system with a state space equation  $x(t)$  that has bounded function  $|f(x)| < f_0$ -constant could have the control signal  $u$ , where  $u$  is given by (1.2).

$$u = \begin{cases} u_o & \text{if } i_L < I_L^* - \Delta i_r^* \\ -u_o & \text{if } i_L > I_L^* + \Delta i_r^* \end{cases} \quad (1.2)$$

$i_L$  is the inductor current and  $u_o$  is a constant dependent on the system dynamic for switching operation such as the logic high and low. Also, the SMC could be represented mathematically as

a relay control as shown in Fig. 5. the condition for making the error reaches zero in a finite time is shown in (1.3).

$$i_L \ddot{i}_L < i_L^* \quad (1.3)$$

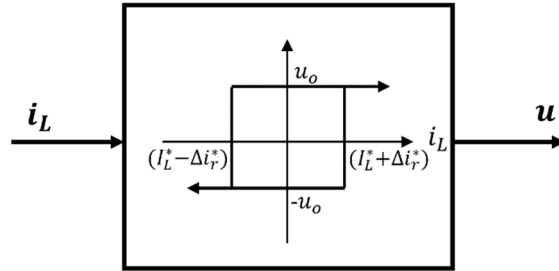


Fig1.3 Sign function (relay control).

The implementation of the SMC is done using hysteresis switching for the inner loop current controller. Thus, the ripple of the inductor current is measured and then compared to the desired ripple based on the reference control signal. The control signal is the result of the outer voltage or current loop controller. A Type three compensator (PID) controller is designed to keep tracking the reference voltage that is controlled using the MPPT algorithm. Accordingly, the transfer function of the compensator is represented in (1.4).

$$G_c(S) = K \times \frac{1 + ST_{z1}}{ST_{z1}} \times \frac{1 + ST_{z2}}{(1 + ST_{p1})(1 + ST_{p2})} \quad (1.4)$$

Where K is the gain, the replica of  $T_{z1}$  and  $T_{z0}$  represent the frequencies of the zeroes. Also, the replica of  $T_{p1}$  and  $T_{p2}$  represent the frequencies of the poles.

#### 1.4 Simulation and Experimental Results

The hysteresis switch could be implemented on PSIM using two comparators and flip flop to achieve the desired logic for gate control. The whole control system is shown in Fig. 1.4.

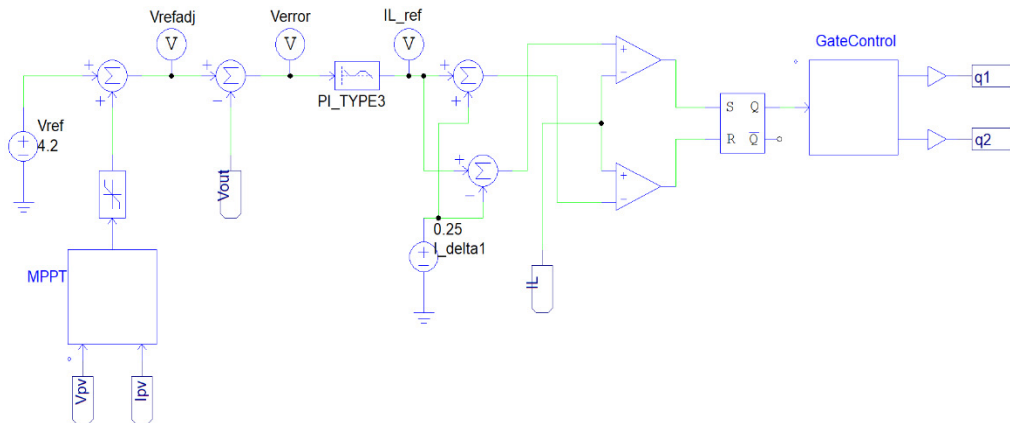


Fig. 1.4 MPPT with a SMC as inner loop current controller

The simulation results for the SMC hysteresis switching control and a regular PID controller are shown in Figures. 1.5-1.8. Fig. 1.5 is the simulated output voltage and power using only a PID controller where column one represents the output voltage (red) with respect to the irradiance (blue). The dotted square waveform represents how slow the system responds to the irradiation and disturbances. While the results are shown in Fig. 1.6 is for the SMC, where it is a way faster to reach the maximum power point, and it's impressively faster to respond to any disturbances that happen on the load or the source.

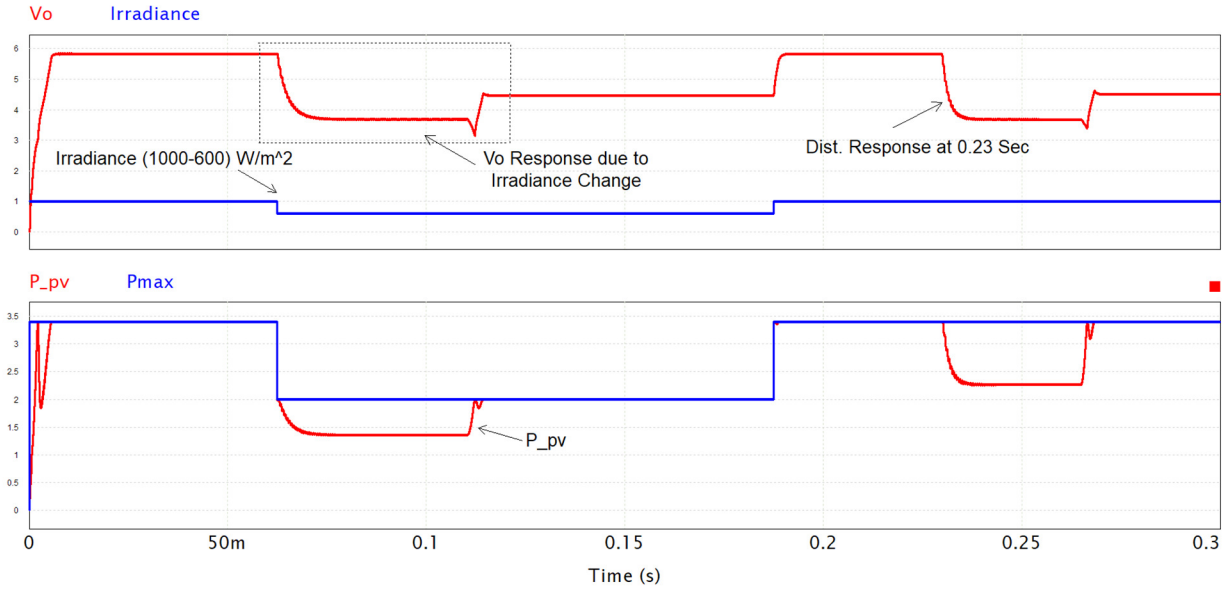


Fig. 1.5.  $V_{out}$ , Irradiance,  $P_{max}$ , and  $P_{PV}$  results using only voltage PID controller.

In addition, Fig. 1.7 shows how the inductor current will be controlled by the hysteresis band that is governed by the desired ripple to improve and stabilize the system responses as in Fig. 1.8. Also, Fig. 1.9 represents the analog implementation of the SMC hysteresis band controller, where  $I_L^*$  is calculated using a programmed PID controller as an output loop on DSP board (F28335).

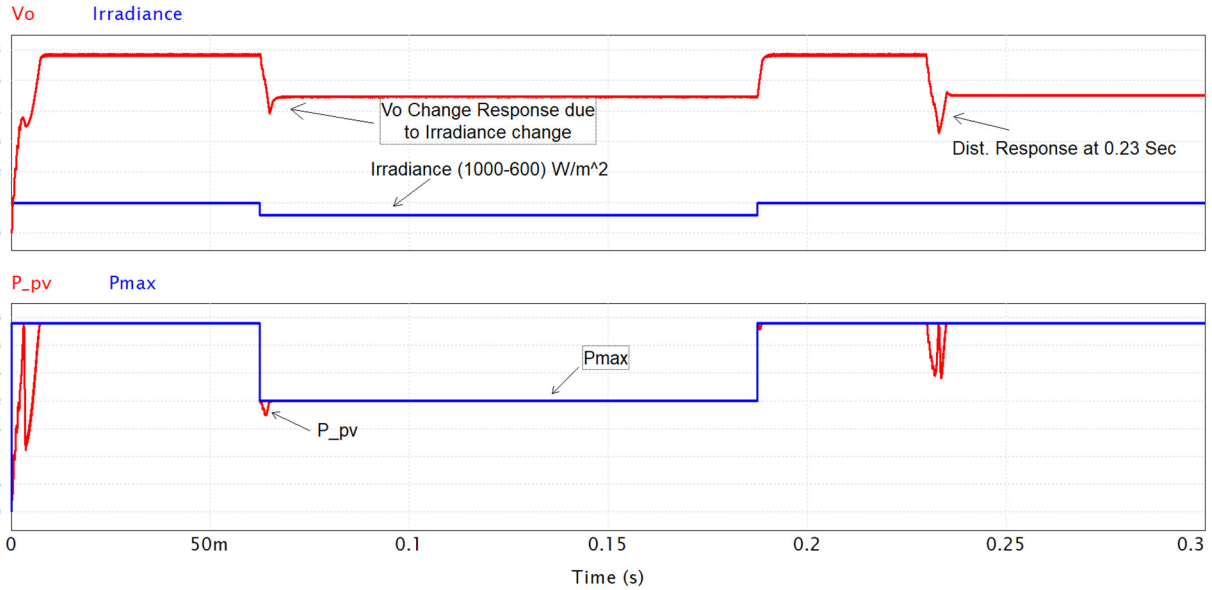


Fig.1.6  $V_{out}$ , Irradiance,  $P_{max}$ , and  $P_{pv}$  results of using voltage controller and SMC current controller.

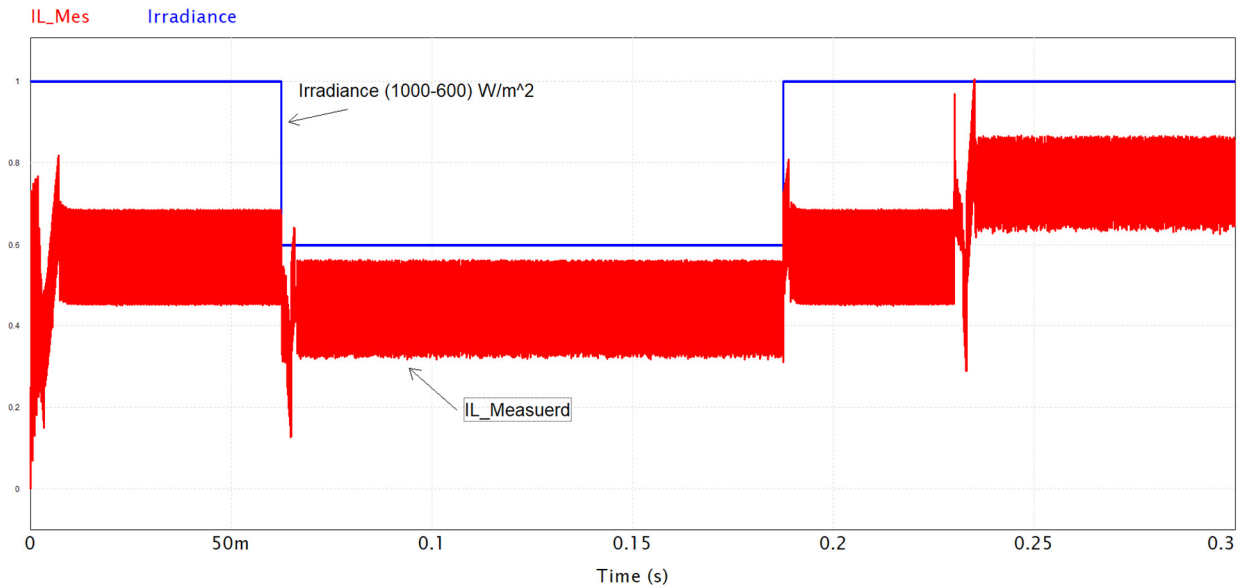


Fig. 1.7 Inductor current with respect to the irradiance.

At last, Fig. 1.10 shows the experimental result of the inductor ripple current with respect to the PWM control that drives the MOSFET. The desired ripple is about 0.2 A, Frequency of 32.89KHz, and duty cycle of 55%. Fig. 1.11 shows the step response of the output current using a PI current controller with hysteresis SMC as an inner control loop. The disturbance is enforced by increasing the load equivalent resistance at the sudden time frame.

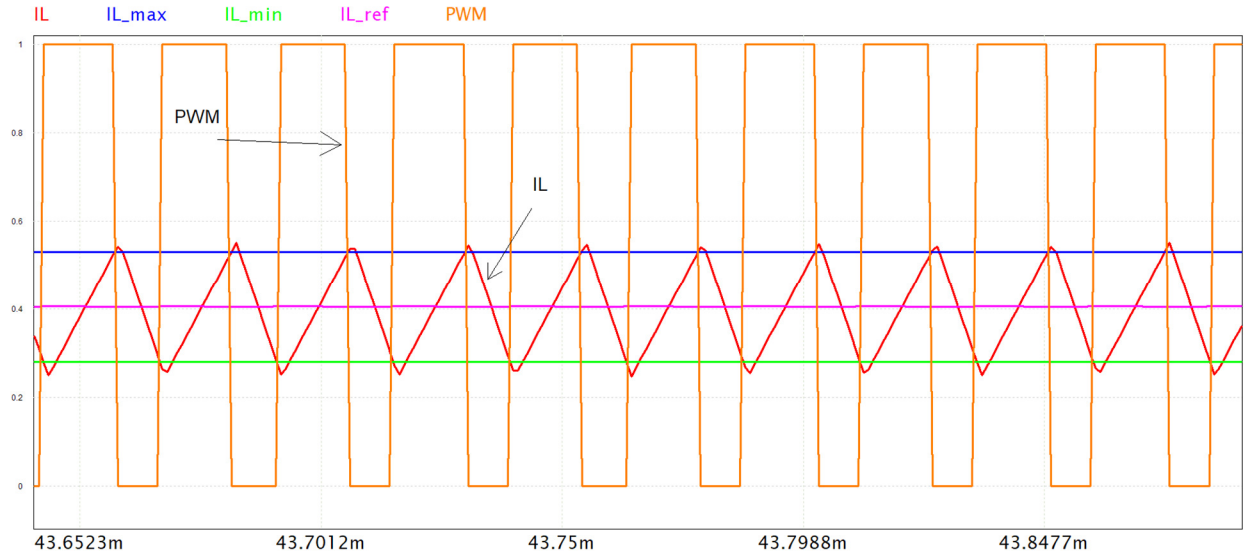


Fig. 1.8 Inductor Current working within the band that tolerate between the reference current

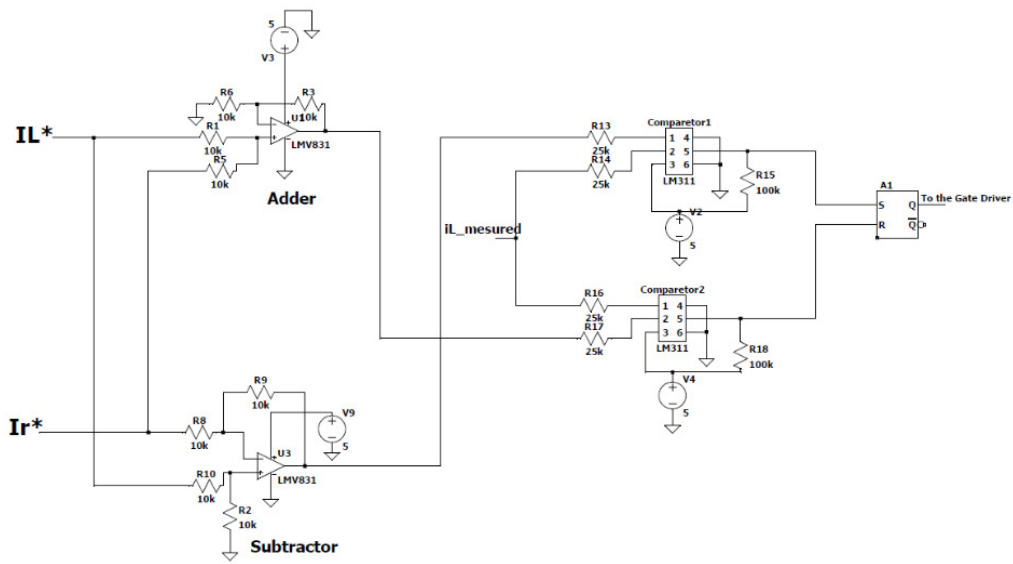


Fig. 1.9 The hysteresis SMC analog implementation.

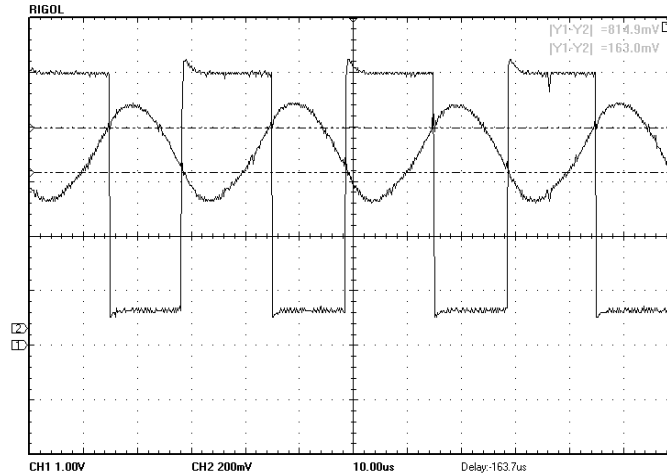


Fig. 1.10 Inductor ripple current with respect to the PWM

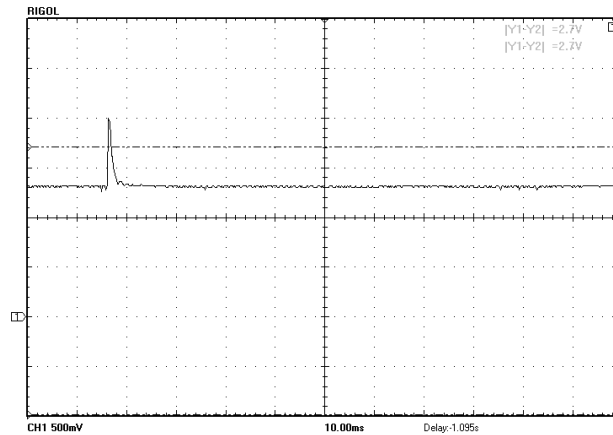


Fig. 1.11 Step response of the output current due to double the load equivalent resistance (

The system works in a more efficient way using SMC as an inner loop current controller. As seen in Fig1.10 that the actual inductor current slides along with the reference current. This means that the error is zero and the system is operating in a steady state. Also, the buck-boost converter is working in CCM in all cases. The SMC has an overall higher efficiency rather than using only a PID voltage controller. Besides, the current overshoot is smaller than that of the regular PID controller, which enhances and protects the component from damages. The efficiency of an ideal component power stage comparison is shown in Table II.

TABLE II. EFFICIENCY CONTROLLER COMPARISON FOR IDEAL COMP.

Controller Type	Efficiency %
PID	99%
PID and SMC	99.63%

### 1.5. Conclusion and Future Works.

The simulation and experimental results show that the proposed prototype system runs effectively. The work done in this research was a very important step in moving toward all renewable energy sources utilization for low power applications. Future works in photovoltaic panels, wind generators, and piezoelectric strings are needed to be analyzed further and then implemented. Also, partial irradiation is needed to be included in the PV system. Correspondingly, a hardware implementation with all energy sources integration will be expected to validate the proposed algorithm.

## 2. Sliding Mode Control Based Battery Management for Energy Harvesting

### 2.1 Battery Management System

The battery management system can manage the charge and discharge status of the battery. Deep discharge and fast recharge can reduce the life expectancy and capacity of the battery [2.1]. The battery management system seen Fig. 2.1. constantly monitors the state of charge (SOC) of the battery to decide whether to charge or stop charging the battery. The monitoring is accomplished by constantly sensing the battery voltage and battery current. Providing a constant current and constant voltage at different states of charge sets the battery charging. The proposed hybrid system for energy harvesting includes a battery management system to improve battery efficiency and its life expectancy by adjusting the charge and discharge rate through a constant voltage and constant current controls.

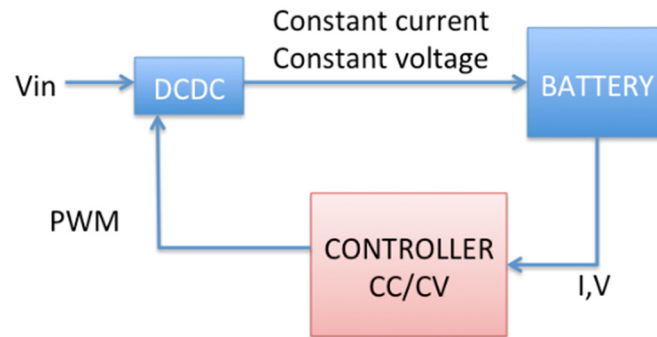


Fig. 2.1 Battery management system

The objective of a battery management system is to control the charge and discharge of a battery. For this research, 3.7 V are targeted at the output to power a wireless sensor network. Therefore, the lithium-ion battery nominal voltage is 3.7V, and the maximum charging voltage is 4.2V. The current during the constant current state of the battery charging is 20% of the battery capacity. The cut-off current during the constant voltage state shall be 1% of the battery capacity. The discharge cut-off voltage for this battery shall be 80% of the nominal voltage, which is 3.0V. If the battery voltage drops far below 3.0V, a preset constant current typically of 10% of the battery capacity is applied to the battery until it reaches a preset voltage of 3.0V.

### 2.2 Constant Current and Constant Voltage Controller

Renewable The purpose of the current and voltage controller is to maintain the current and voltage constant. This is accomplished by adjusting the PWM duty cycle going into the gate of MOSFET in the DC-DC converter; refer to Fig. 2.2 [2.2] for the charging scheme. Fig. 2.3 [2.3] represents the battery charging control algorithm based on the constant current (CC)/constant voltage (CV) [2.4] charging scheme. The algorithm does not allow charging on the battery if the DC bus is not greater than 4.2V/0.8. The controllers will take place at different times based on the

charging control algorithm. The input voltage is based on the output rated voltage of the PV cell (7V, 3.4W). Thus, a buck converter is used to step down the voltage to 4.2 volts. Also, the duty cycle is limited between 20% and 80% to avoid stress on the MOSFET.

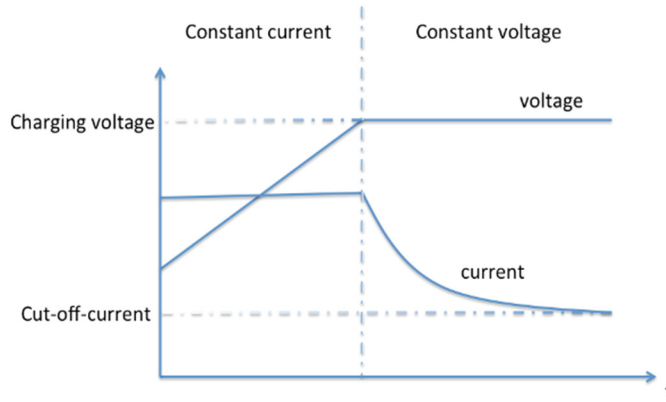


Fig. 2.2 CC/CV charging scheme

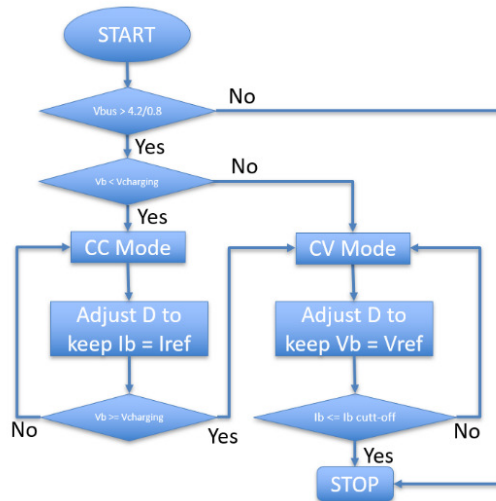


Fig. 2.3 Charging control algorithm

### 2.2.1 Constant Voltage Controller

Most of the time to improve the performance of a PID(Proportional Integral Derivative) controller, the switching frequency could increase [2.5]. The constant voltage feedback control loop consists of a PI(Proportional Integral) controller, which can provide zero state error. A general PI controller is implemented based on the equation (2.1)

$$\frac{V_c(s)}{e(s)} = K_p \frac{s+K_i/K_p}{s} \quad (2.1)$$

Where  $K_p$ , and  $K_i$  are the gains of the PI controller and  $s$  is the Laplace operator

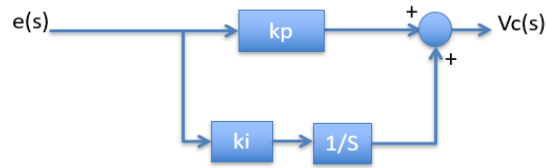


Fig 2.4 PI controller for constant voltage

### 2.2.2 Constant Current Controller

The current controller is designed using robust sliding mode control (SMC). The state equations for the buck converter are shown in equations (2.2~2.3) [2.6].  $E$  is the input voltage,  $V_o$  is the output voltage,  $L$  is the inductance,  $C$  and  $R$  are the capacitance and resistance. The variable  $u$  is the control input taking discrete values of 0 and 1 [2.6]. These state equations are obtained by doing a dynamic analysis on the buck converter.

$$\frac{di_L}{dt} = \frac{E}{L}u - \frac{V_o}{L} \quad (2.2)$$

$$\frac{dV_o}{dt} = \frac{i_L}{C}u - \frac{V_o}{RC} \quad (2.3)$$

Fig. 2.5 represents the feedback controller with SMC of the buck converter based on the above state equations. To design the SMC the error is defined as  $X_1$  and  $V_o$  is defined as  $X_2$ .  $V_i$  is the voltage at the DC bus. Also Fig. 2.6 shows Simulink SMC implementation.

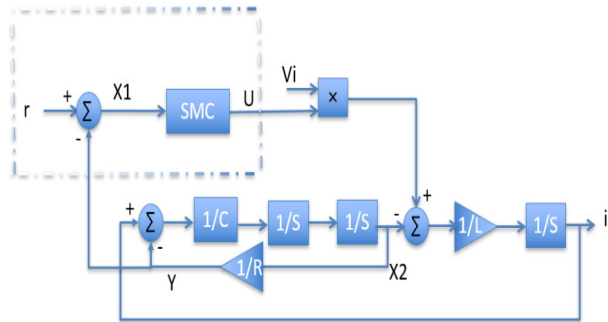


Fig. 2.5 Buck converter block diagram representation with SMC controller

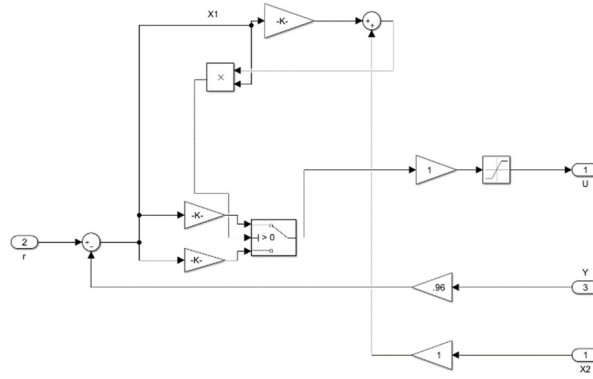


Fig. 2.6 Simulink SMC controller implementation

### 2.3. Simulation and Experimental Results

The overall battery management system is shown in Fig. 2.7. As can be seen in Fig. 2.8, it takes 10ms for the current controller to match the 240mA reference current. After that, the current is constant until the battery voltage is 4.2V. At that point, the voltage is kept constant until the battery current becomes 12mA. When the cut-off current condition is met, the battery is disconnected from the circuit. Fig. 2.9 shows the result of the fuzzy versus SMC current controller, which was analyzed to compare their performances. As can be seen in Fig. 2.9, the SMC controller tracks the 240mA reference current more accurately than the fuzzy controller.

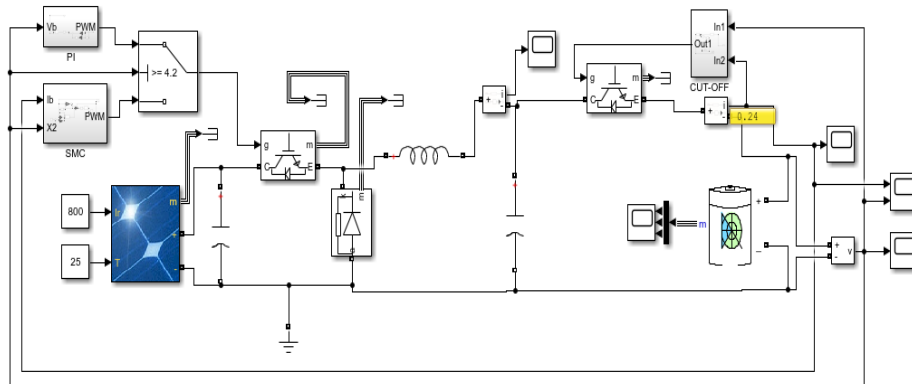


Fig. 2.7 Battery management system

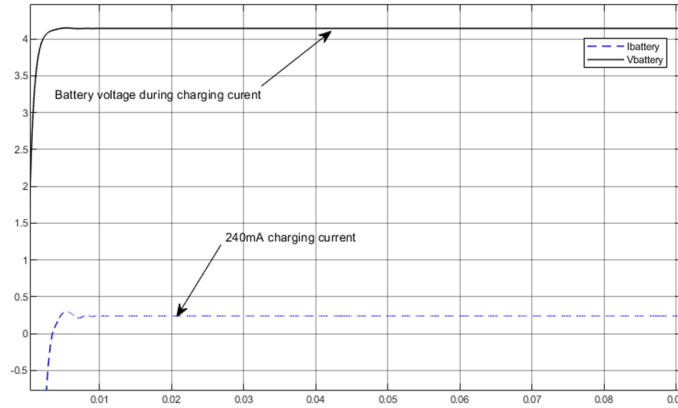


Fig. 2.8  $I_b$  CC and  $V_b$  during charging state

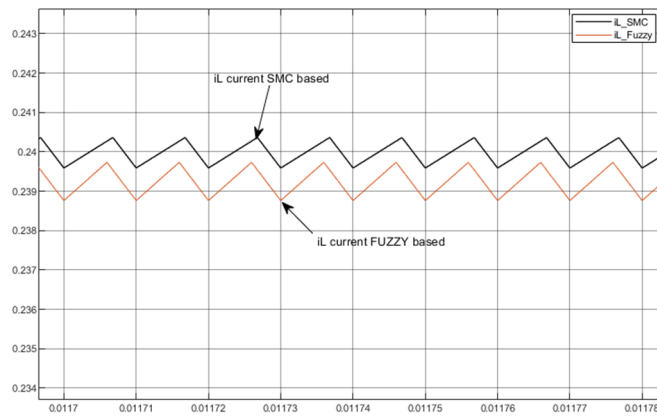


Fig. 2.9  $i_{L\_Fuzzy}$  Vs  $i_{L\_SMC}$

The battery management system has been tested using the TI Delfino F28335. Table III, and IV indicates the specifications of the buck converter components, PV panel, and battery used. Note that the current reference in the actual experiment is limited to 230mA due to the current limitations of the electrical rating of some components, such as the inductor.

TABLE III. BUCK-CONVERTER COMPONENTS VALUE

Capacitor value to clean PV voltage noise	1000uF
Capacitor value at the output	1000uF
Inductor	1mH

TABLE IV. PV PANEL RATING

Output Power	6W
Isc	930mA
Voc	6V

TABLE V. LITHIUM -POLYMER BATTERY RATING

Capacity	1200mA
Nominal voltage	3.7V
Voltage at end of discharge	3.0V
Charging voltage	4.2V

Fig.2.10 shows the DSP reading of the constant charging current of 230mA. On the other hand, Fig. 2.11 shows the voltage at the battery during the constant current charging state. As can be seen the voltage at the battery is increasing and the current begins to decrease once the battery reaches 4.2V. This is because at this point the battery is charging based on a constant voltage.

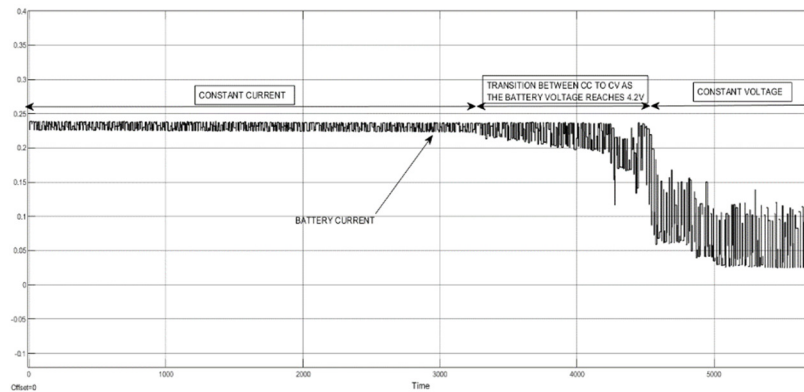


Fig. 2.10 Experimental battery current

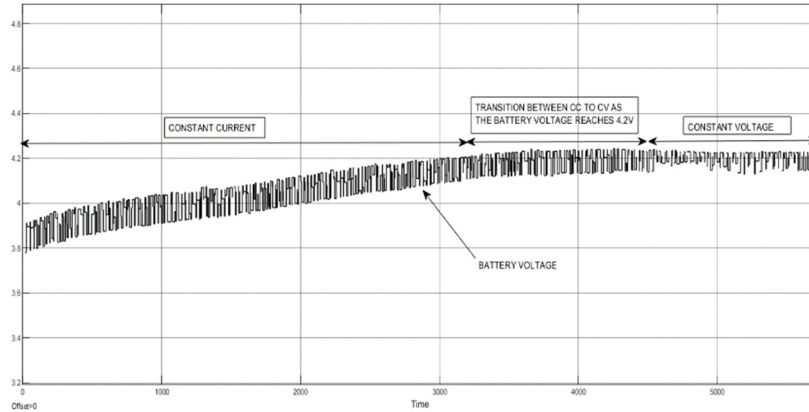


Fig. 2.11 Experimental battery voltage

## 2.4 Conclusion and future works

Overall, the system simulation reflected the constant current and constant voltage charging states. The controllers were able to track the 4.2V reference and the 240mA reference. In comparison to the Fuzzy controller, the SMC controller provided a smaller error, being more robust; however, the fuzzy has a better response time. The experimental results show that the SMC controller tracks the 230mA reference current during the constant current charging state with very little error, with a 10mA above and below the specified reference current. Note that during the constant voltage charging state, the voltage at the battery is maintained at 4.2V as expected. More robust experimental tests with ultracapacitor will be expected during 2020~2021.

### 3. Development of Artificial Neural Network Based Maximum Power Point Tracking Algorithm for a Photovoltaic Application

During 2019~2020, an artificial neural network (ANN) is being also investigated to improve the efficiency of the maximum power point tracking (MPPT) algorithm in a photovoltaic (PV) application. The data used in this proposed ANN training are obtained from a fuzzy logic controller in the buck converter connected to a PV panel. The use of the combined ANN and the fuzzy logic controller allowed the PV system to operate at its maximum power point in both full and partial radiation conditions more efficiently compared to conventional algorithms such as perturb and observe (P&O), incremental conductance (IC), and genetic algorithms.

#### 3.1 Artificial Neural Network(ANN) based MPPT

The proposed solution in this research is to combine the fuzzy logic controller MPPT algorithm with the artificial neural network (ANN). By using the data, two inputs and one output, from the fuzzy logic controller to train the artificial neural network algorithm. This approach allowed the ANN MPPT algorithm to reduce the error from the fuzzy logic controller. In this research feedforward backpropagation network ANN is used and in Fig.3.1 shown a typical structure of it.

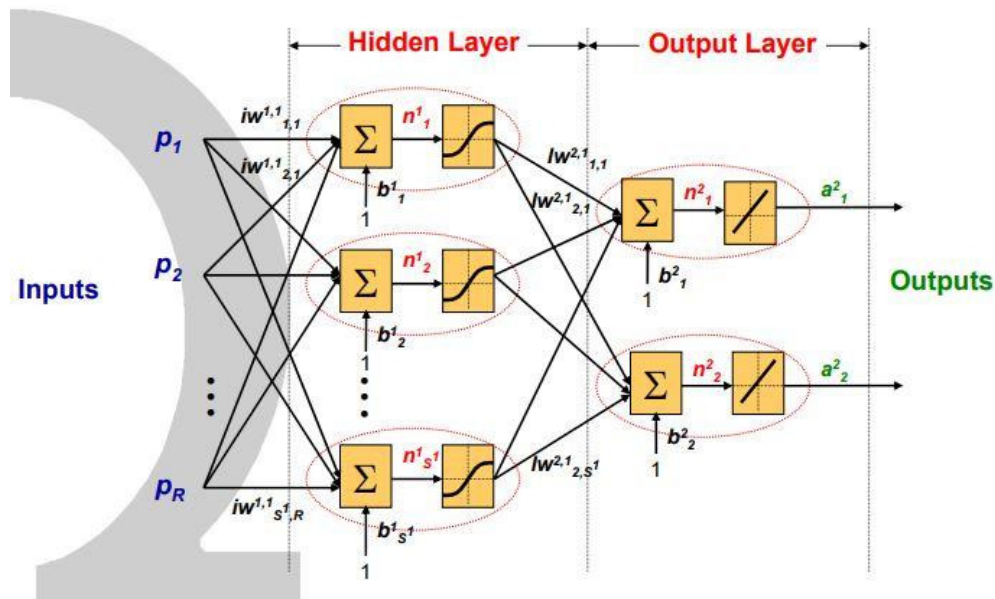


Fig.3.1 ANN - Feedforward backpropagation network [3.8]

There are three main components of the feedforward backpropagation network seen in Fig.3.1, input layer, hidden layer, and output layer. The input layer where inputs from a system are fed into the hidden layer. In the hidden layer, the inputs are processed through inter-unit connection strengths or weights. Where the weights are determined by a process of adaptation, or learning from a set of training patterns [3.8]. In a feedforward backpropagation network, the weights and

biases of the neural network are updated by using a variety of gradient descent algorithms [3.8]. A feedforward backpropagation (BP) network was chosen for this PV system with partial shading MPPT, because of its abilities to solve the nonlinear system. This is useful because the PV system is a sporadic system when it is experiencing weather changes. Furthermore, a feedforward BP network is capable of producing reasonable results on inputs it has never seen as long as the new inputs are similar to the training inputs [3.8].

### 3.2 Simulation results

Three different simulations are analyzed. The photovoltaic application with Perturb and Observe (P&O), Fuzzy Logic Control (FLC), and Artificial neural network (ANN) MPPT algorithm are simulated. The circuit schematics and results are shown below.

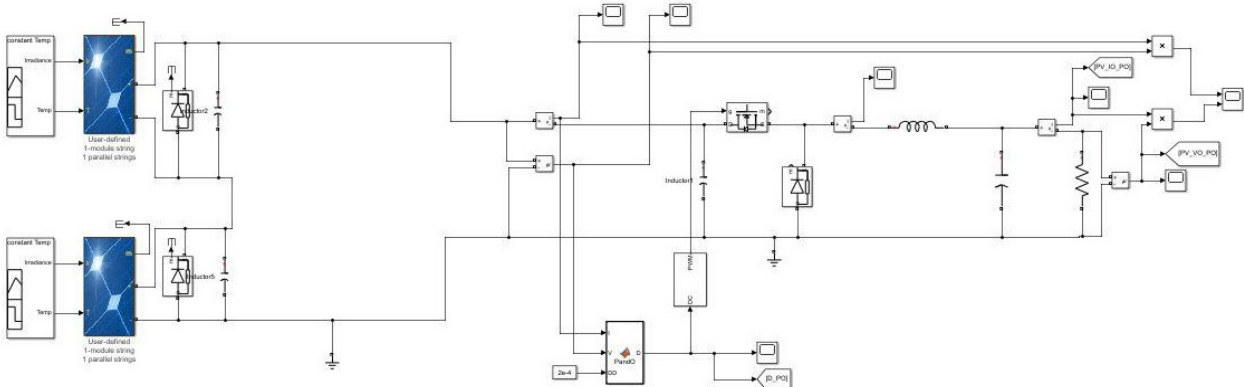


Fig. 3.2 Perturb and Observe MPPT Algorithm

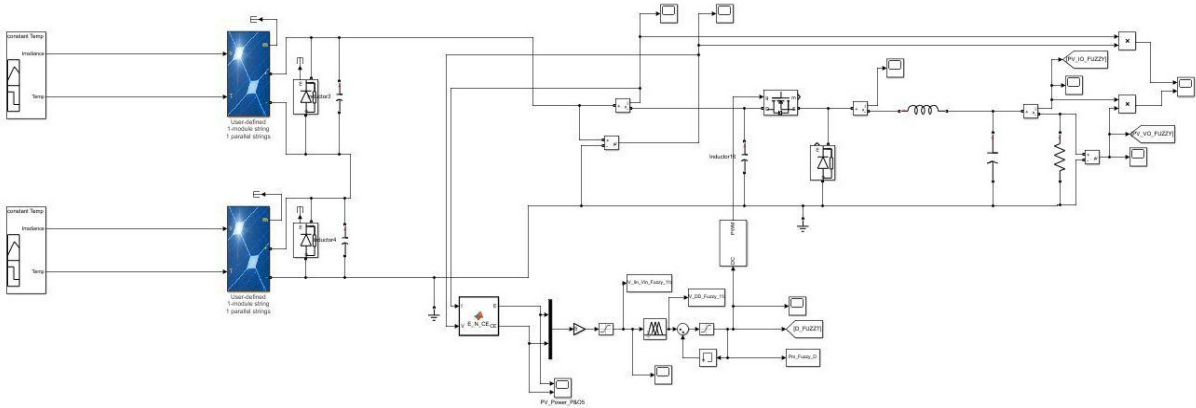


Fig. 3.3 Fuzzy Logic Control MPPT Algorithm

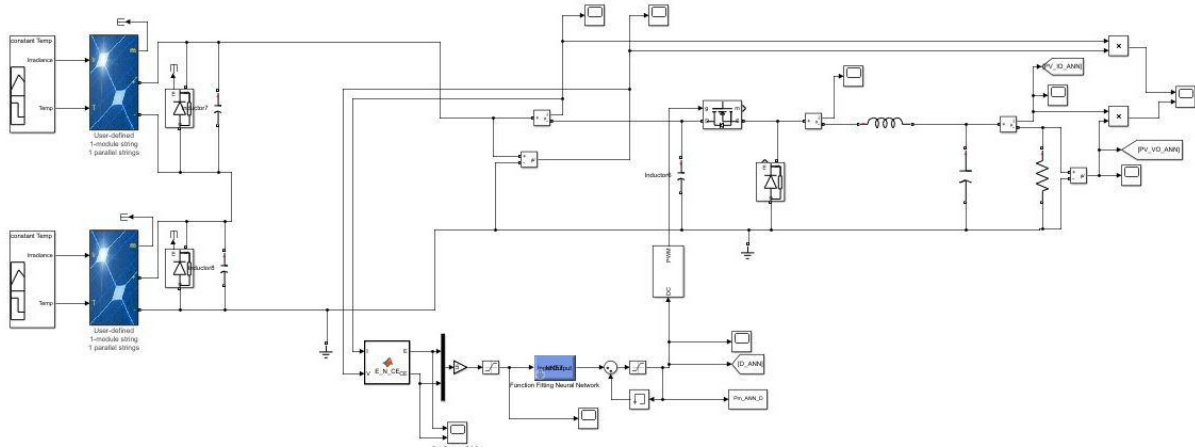


Fig. 3.4 Artificial Neural Network MPPT Algorithm

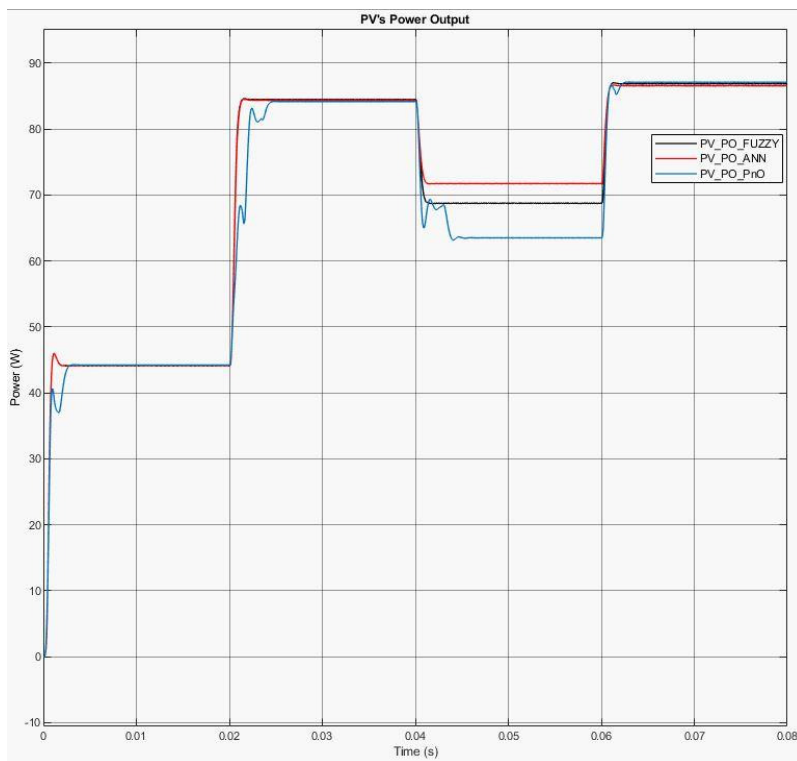


Fig. 3.5 PV Power Output

The simulation results have shown that the P&O MPPT algorithm had a slower response compared to the FLC and ANN MPPT algorithm as shown in Fig. 3.5. However, the P&O is more efficient than FLC MPPT algorithm due to FLC has a greater error rate. But, when ANN MPPT algorithm is used to reduce the error rate from the FLC, the efficiency of the PV application from this algorithm was most improved seen in Fig. 3.5.

The simulation results have shown that the P&O MPPT algorithm had a slower response compared to the FLC and the ANN MPPT algorithm as shown in Fig. 3.5. Furthermore, the FLC MPPT algorithm is more efficient than the P&O MPPT algorithm, because, with the FLC, the duty cycle was responding to the changes of irradiation faster than P&O. The proposed ANN MPPT algorithm was used to reduce the error rate from the FLC, the efficiency of the PV system from this algorithm was most improved seen in Fig. 3.5.

### 3.3 Conclusion and future works

Photovoltaic application is a nonlinear system. The three simulated MPPT algorithms demonstrated that each algorithm operated at different power output efficiency. The results show that the proposed artificial neural network was the most efficient. The work done in this research was a very important step of moving toward higher usage of renewable energy sources. This research demonstrated that the artificial neural network based MPPT algorithm can be used to improve the efficiency of a photovoltaic application. For 2020~2021, we will push forward to implement the proposed ANN MPPT into our actual energy harvesting system.

## References

- [1.1] Vaduim Utikan, Jurgen Guldner, Jingxin Shi, "Sliding Mode Control in Electromechanical Systems" 1999 ISBN-0-7484-0116-4.
- [2.1] N. K. Raghavendra and K. Padmavathi, "Solar Charge Controller for Lithium-Ion Battery," *2018 IEEE International Conference on Power Electronics, Drives and Energy Systems (PEDES)*, Chennai, India, 2018, pp. 1-5.
- [2.2] Leemput, Niels. (2015). Grid-supportive Charging Infrastructure for Plug-in Electric Vehicles
- [2.3] Khan, Wajahat & Ahmad, Furkan & Alam, Mohammad. (2018). Fast EV charging station integration with grid ensuring optimal and quality power exchange. *International Journal of Engineering Science*. 1-10. 10.1016/j.jestch.2018.08.005.
- [2.4] Weixiang Shen, Thanh Tu Vo and A. Kapoor, "Charging algorithms of lithium-ion batteries: An overview," *2012 7th IEEE Conference on Industrial Electronics and Applications (ICIEA)*, Singapore, 2012, pp. 1567-1572. doi: 10.1109/ICIEA.2012.6360973
- [2.5] L. Dinca and J. Corcau, "P.I. versus fuzzy control for a DC to DC boost converter," *2016 International Symposium on Power Electronics, Electrical Drives, Automation and Motion (SPEEDAM)*, Anacapri, 2016, pp. 803-808
- [2.6] nullH. Guldemir, "Study of Sliding Mode Control of DC-DC Buck Converter," *Energy and Power Engineering*, Vol. 3 No. 4, 2011, pp. 401-406. doi: [10.4236/epe.2011.34051](https://doi.org/10.4236/epe.2011.34051).
- [3.1] S. Khadidja, M. Mountassar and B. M'hamed, "Comparative study of incremental conductance and perturb & observe MPPT methods for photovoltaic system," *2017 International Conference on Green Energy Conversion Systems (GECS)*, Hammamet, 2017, pp.
- [3.2] B. Subudhi and R. Pradhan, "A Comparative Study on Maximum Power Point Tracking Techniques for Photovoltaic Power Systems," in *IEEE Transactions on Sustainable Energy*, vol. 4, no. 1, pp. 89-98, Jan.2013. doi: 10.1109/TSTE.2012.2202294
- [3.3] K. Amara et al., "Improved Performance of a PV Solar Panel with Adaptive Neuro Fuzzy Inference System ANFIS based MPPT," *2018 7th International Conference on Renewable Energy Research and Applications (ICRERA)*, Paris, 2018, pp. 1098-1101.
- [3.4] H. H. Lee, L. M. Phuong, P. Q. Dzung, N. T. Dan Vu and L. D. Khoa, "The new maximum power point tracking algorithm using ANN-based solar PV systems," *TENCON 2010 - 2010 IEEE Region 10 Conference*, Fukuoka, 2010, pp. 2179-2184.
- [3.5] M. F. Nayan and S. M. S. Ullah, "Modelling of solar cell characteristics considering the effect of electrical and environmental parameters," *2015 3rd International Conference on Green Energy and Technology (ICGET)*, Dhaka, 2015, pp. 1-6, doi: 10.1109/ICGET.2015.7315096.
- [3.6] Daniel W. Hart, *Power Electronics*, McGraw-Hill, 2011, pp. 198–205.
- [3.7] Bendib, B., et al. "Advanced Fuzzy MPPT Controller for a Stand-Alone PV System." *Energy Procedia*, vol. 50, 2014, pp. 383–392., doi:10.1016/j.egypro.2014.06.046.

[3.8] “Statistics & Data Analysis Using Neural Network.”  
doi:[https://www.academia.edu/34793472/Statistics\\_and\\_Data\\_Analysis\\_using\\_Neural\\_Network\\_Copyrighted\\_2005\\_TechSource\\_Systems\\_Sdn\\_Bhd\\_1\\_Statistical\\_and\\_Data\\_Analysis\\_Using\\_Neural\\_Networ](https://www.academia.edu/34793472/Statistics_and_Data_Analysis_using_Neural_Network_Copyrighted_2005_TechSource_Systems_Sdn_Bhd_1_Statistical_and_Data_Analysis_Using_Neural_Networ).

# Appendix A

Figure A1.1: Solar and Wind Eagle Software Schematic

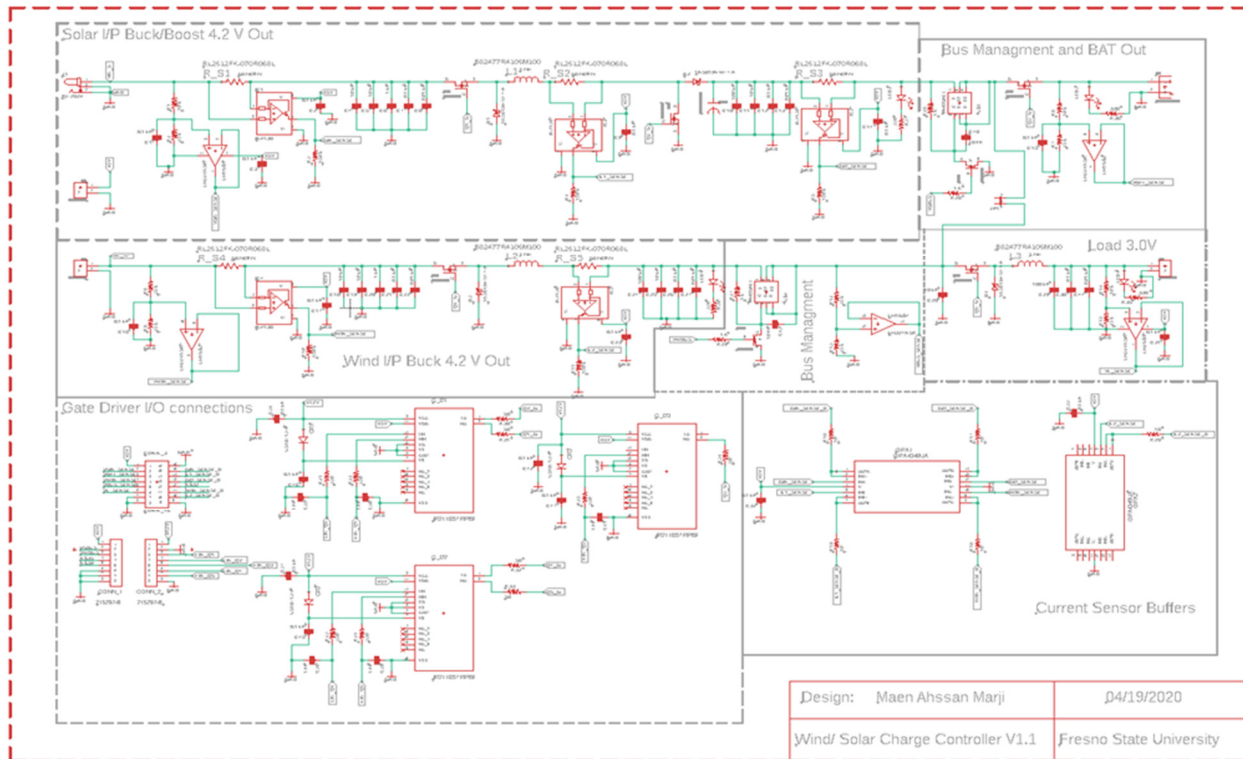


Figure A1.2: PCB Printed Board manufacturing top layer preview

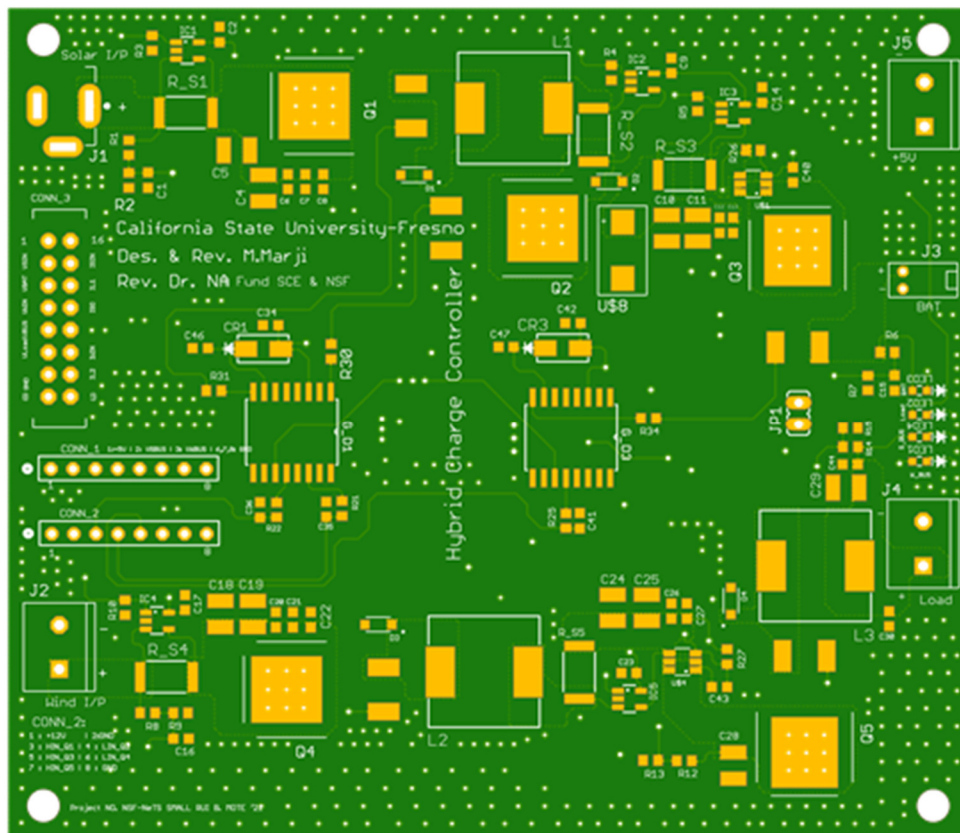


Figure A1.3: PCB and The analog implementation of the hysteresis band SMC current controller

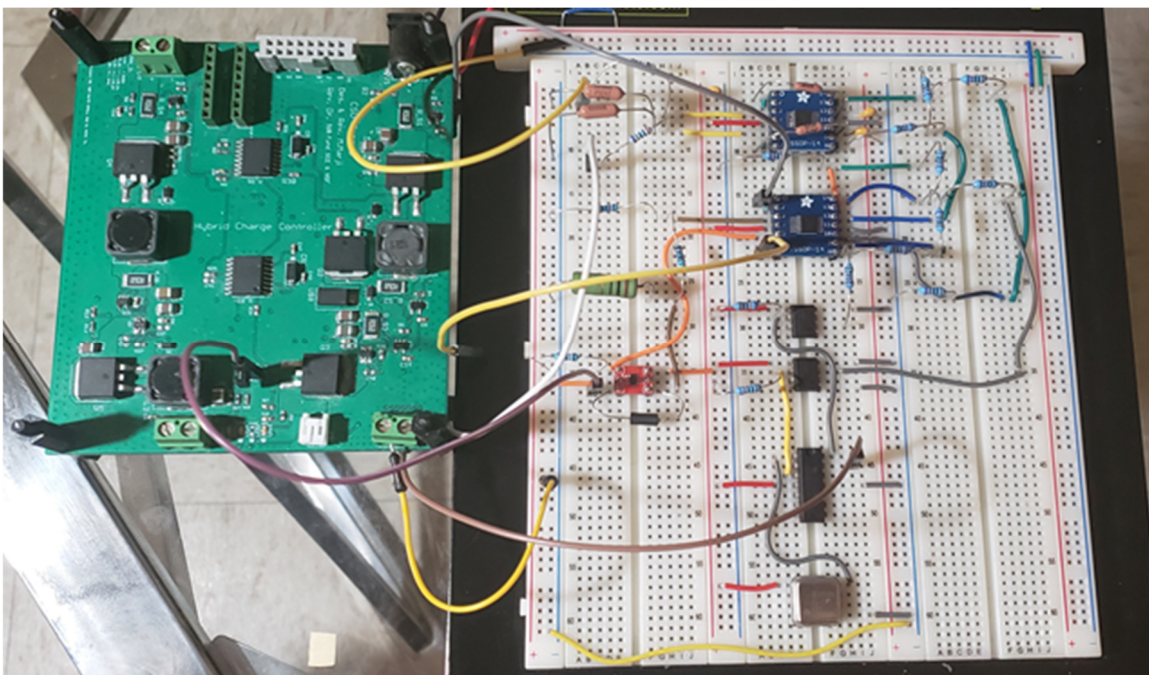


Figure A.1.4: Matlab Embedded Software with the F28335 DSP development board.

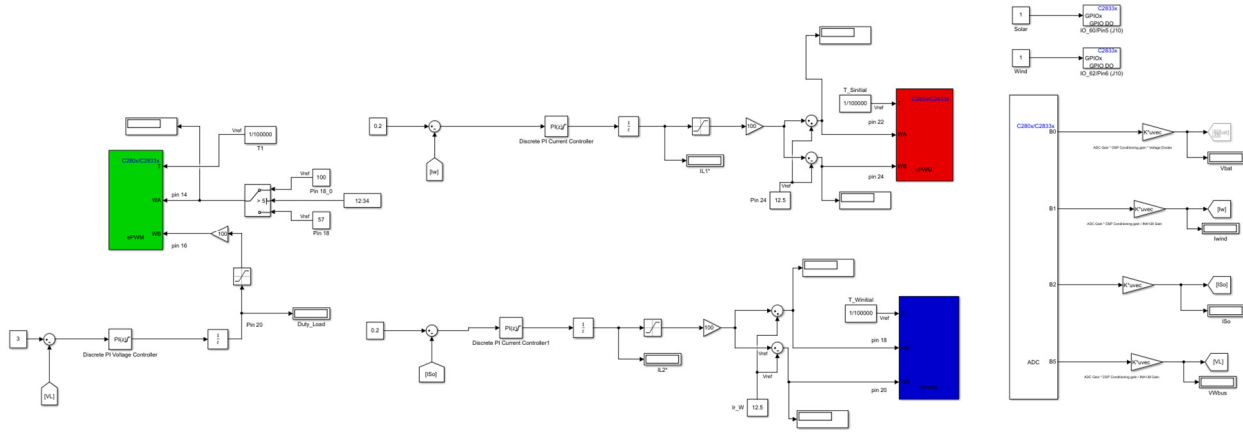


Figure A2.1 CIRCUIT BOARD: Bidirectional Battery management system with supercapacitor

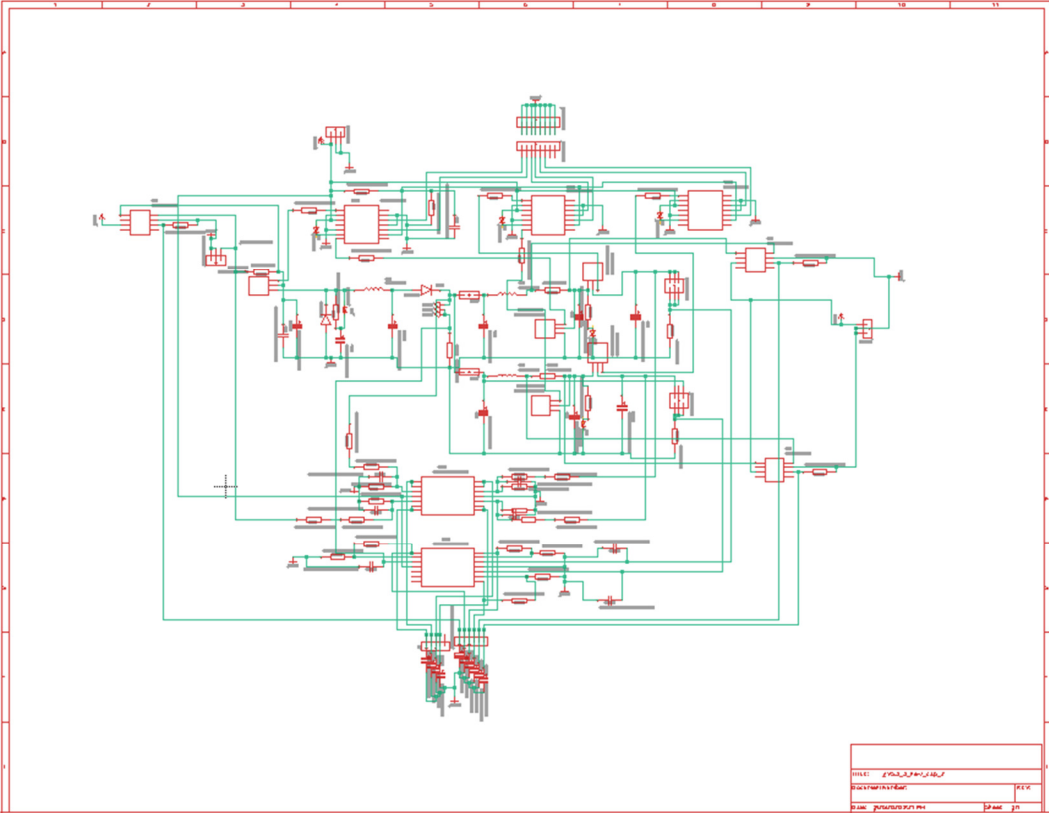
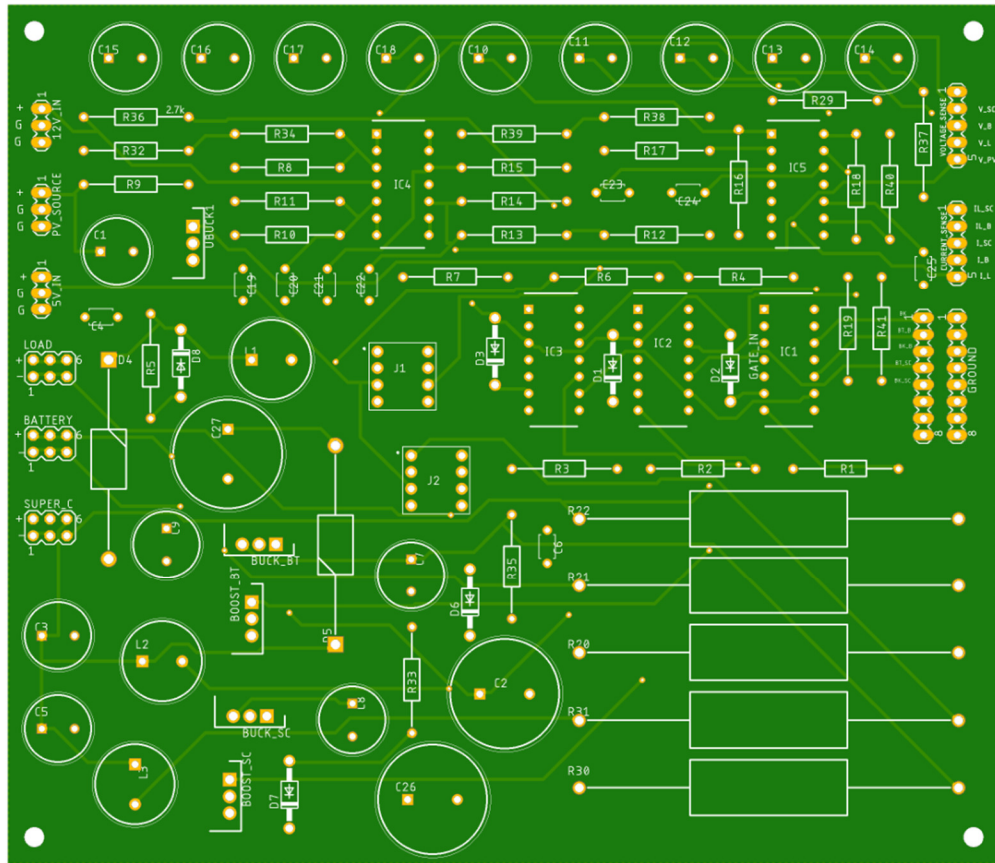


Figure A2.2 PCB BOARD: Bidirectional Battery management system with supercapacitor



### A3.1 Perturbed and Observed Matlab Code:

```

function D = PandO(Param, V, I)
% *****
% MATLAB implementation of a Perturb and Observe algorithm
% for Maximum Power Point Tracking. This algorithm is designed
% to operate with a buck converter
%
% Created by: Carlos Osorio
% Modified by Cheaheng Lim (9-26-2020)
%*****

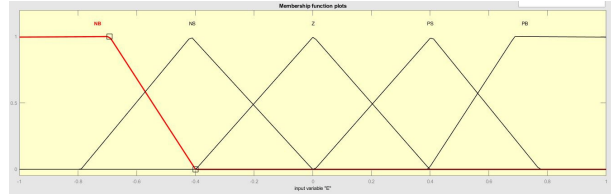
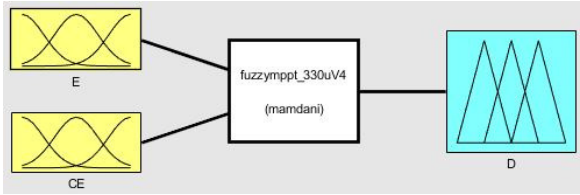
% D output = Duty cycle (value between 0 and 1)
% V input = PV array terminal voltage (V)
% I input = PV array current (A)

% Param input:
Dinit = Param(1); %Initial value for D output
Dmax = Param(2); %Maximum value for D
Dmin = Param(3); %Minimum value for D
deltaD = Param(4); %Increment value used to increase/decrease the duty cycle D
% Set up the local variables
persistent Vold Pold Dold Fmpp;
% If Vold is empty then set the local variables as follow
if isempty(Vold)
    Vold=0;
    Pold=0;
    Dold=Dinit;
    Fmpp=0;
end
% Calculate measured array power
P= V*I;
dV= V - Vold;
dP= P - Pold;
% Increase or decrease duty cycle based on conditions
if P<Fmpp
    if dP < 0
        if dV < 0
            D = Dold - deltaD;
        else
            D = Dold + deltaD;
        end
    else
        if dV < 0
            D = Dold + deltaD;
        else
            D = Dold - deltaD;
        end
    end
else
    D=Dold;
end
% Limit the duty cycle boundary
if D >= Dmax || D<= Dmin
    D=Dold;
end
% Reset the present values to the previous Values
Dold=D;
Vold=V;
Pold=P;
Fmpp=P;
end

```

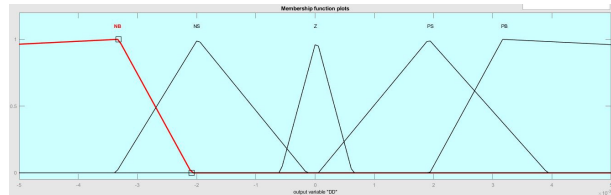
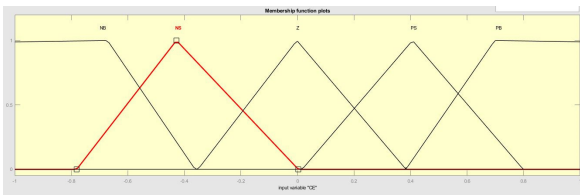
A.3.2 Figure A3.1 (a) is the Fuzzy Layout; (b) is the Fuzzy “E” input; (c) is the fuzzy “CE” input; (d) is the Fuzzy “DD” output; (e) is the Fuzzy’s rules.

Figure A3.2 (a) is the Fuzzy Layout; (b) is the Fuzzy “E” input; (c) is the fuzzy “CE” input; (d) is the Fuzzy “DD” output; (e) is the Fuzzy’s rules.



(a)

(b)



(c)

(d)

TABLE IV. FUZZY'S RULES

E/CE	NB	NS	Z	PS	PB
NB	PB	PB	PS	NS	NB
NS	PS	PS	PS	NB	NS
Z	PS	PS	Z	NS	NS
PS	PS	PS	NS	NS	NS
PB	PS	PS	NS	NS	NS

(e)

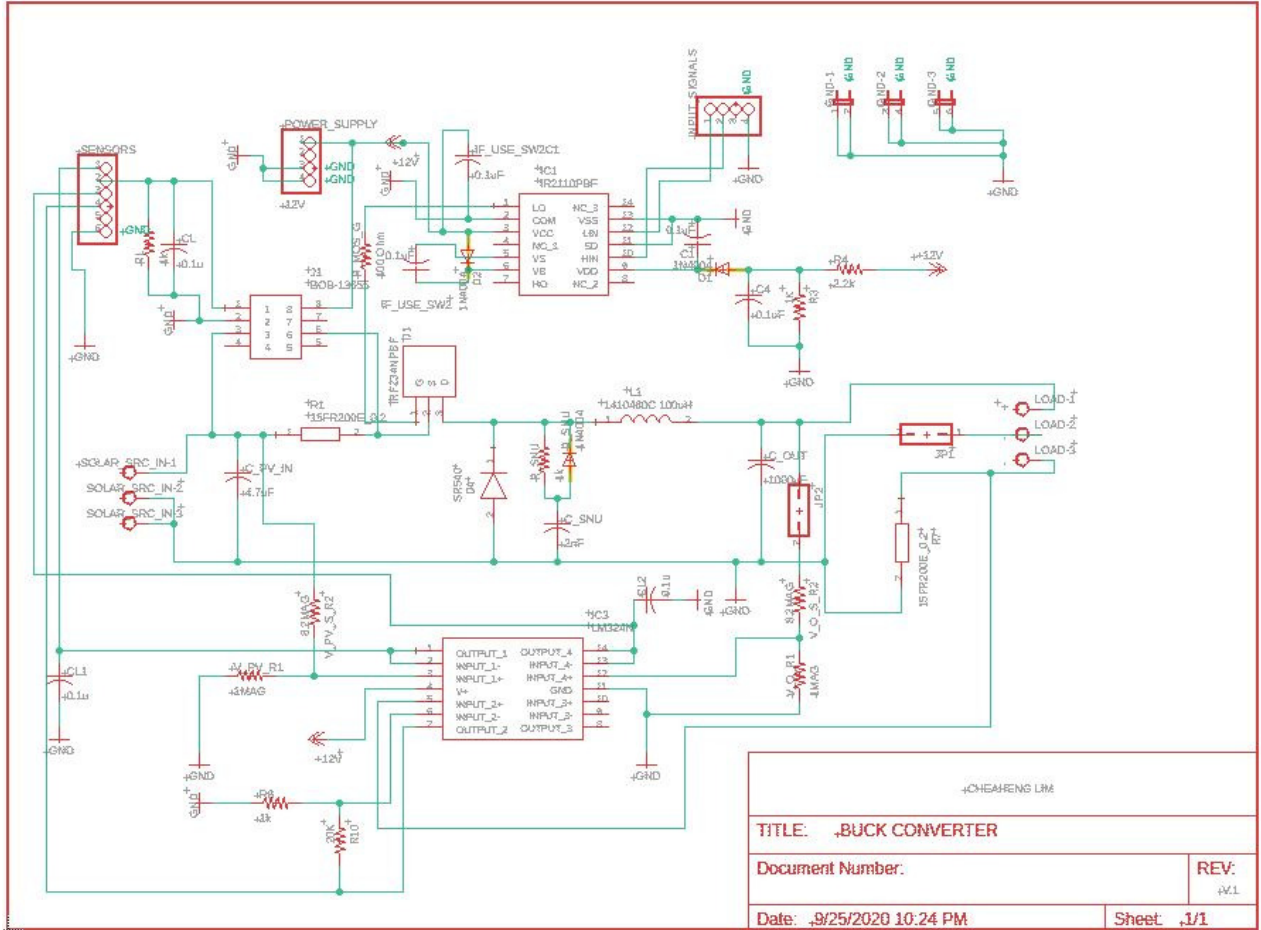


Figure A3.3 Buck Converter PCB Schematic

